MRAS Observers for Doubly-Fed Induction Machine in Wind Energy Conversion Systems

Kris Scicluna [#1], Cyril Spiteri-Staines [#2], Maurice Apap [#3]

[#] *Dept. of Ind. Electrical Power Conversion*
University of Malta, Msida, MSD 2080
[1] kris.scicluna@um.edu.mt
[2] cyril.spiteri-staines@um.edu.mt

Abstract – **This paper presents the study of a sensorless speed controlled Doubly-Fed Induction Machine (DFIM) using a Model Reference Adaptive System (MRAS). Various Stator Flux Voltage Models found in literature were implemented on a DFIM driven by a rotor side matrix converter. Simulation results for the sensorless closed loop control are presented in the range of operation of a typical wind turbine and rotor angle/speed estimates are presented for each of the Voltage Models.**

Keywords: MRAS, Sensorless, DFIM, Voltage Model, WECS

I. Introduction

The most widespread machines used for wind energy are of the Doubly-Fed Induction Machine (DFIM) type [1]. There are several advantages in using a variable speed system over other machine configurations which include: increased turbine energy capability; reduced stresses on the mechanical structure and diminished acoustic noise [2].

DFIMs are typically controlled through vector control which requires information about the rotor angular position and speed which is usually provided via a speed sensor. Moreover the latter is usually fragile and requires extra electronics for operation. The aim of sensorless algorithms is to provide a speed estimate using a kind of speed observer. The advantages of sensorless techniques include improved system reliability, robustness and reduction in cost [3]. The Model Reference Adaptive System (MRAS) is a model-based sensorless technique which can be implemented on most vector controlled DFIM setups without the need for additional hardware.

This paper aims to simulate a DFIM Stator Field Orientation (SFO) vector control environment with a MRAS. The experimental set-up including the DFIM, whose parameters are shown in Table II and on which sensorless techniques were implemented is shown in Fig. 1 [4-6].

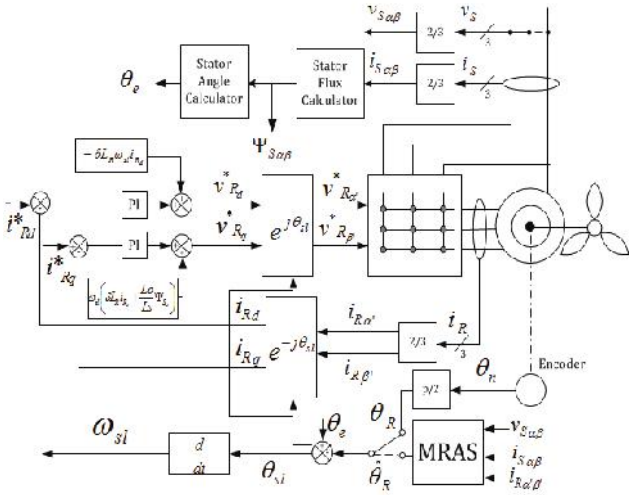

Fig. 1. SFO vector control environment with MRAS

II. MRAS Observer Design

The MRAS mathematical model is based on the work of Schauder [7] and its adaptation to the DFIM is discussed in Cardenas et al. [8-10]. The MRAS observer is shown in Fig. 2 and is based on two models:

1) Voltage Model

2) Current Model

The voltage model is expressed as:

$$\Psi_{S_{\alpha\beta}} = \int v_{S_{\alpha\beta}} - R_S i_{S_{\alpha\beta}} dt \qquad (1)$$

Current model is expressed as:

$$\hat{\Psi}_{S_{\alpha\beta}} = L_S i_{S_{\alpha\beta}} + L_O i_{R_{\alpha'\beta'}} e^{j\hat{\theta}_R} \qquad (2)$$

Where $v_{S_{\alpha\beta}}$ and $i_{S_{\alpha\beta}}$ are the stator voltage and current in the stationary αβ-frame, R_S is the stator resistance, L_S is the stator self-inductance, L_O is the mutual inductance and $\hat{\theta}_R$ is the estimated rotor angle.

The reference and estimated fluxes are compared and an error term ε in the **αβ**-frame is calculated.

$$\varepsilon = \hat{\Psi}_{S_\alpha} \Psi_{S_\beta} - \Psi_{S_\alpha} \hat{\Psi}_{S_\beta} \qquad (3)$$

The error term ε is passed through a proportional integral (PI) controller as shown in Fig. 2 to yield the estimated rotor frequency $\hat{\omega}_R$ and rotor angle $\hat{\theta}_R$. These estimates can be used to operate the vector control scheme replacing the speed sensor.

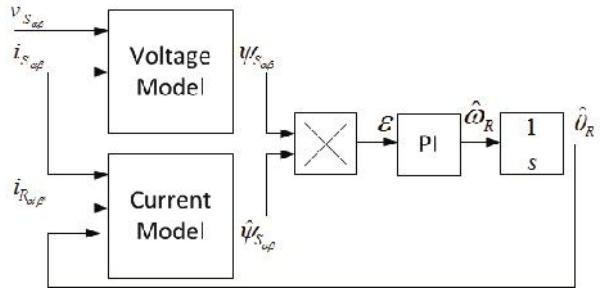

Fig. 2. MRAS Observer

The modelling of the MRAS system is discussed in detail in [8], the authors also explain the tuning of the PI which was applied in the work presented here. Grid-connected operation is assumed with the magnetization current being supplied through both the stator and the rotor. The linearized plant seen by the PI controller is expressed as:

$$G_{MRAS}(s) = \frac{\Delta\varepsilon}{\Delta\omega_R - \Delta\hat{\omega}_R} = \frac{\left(\Psi_{S_{d0}} Lo\, i_{R_{d0}}\right)}{s} \qquad (4)$$

Where $\Psi_{S_{d0}}$ and $i_{R_{d0}}$ are the stator flux and rotor current at the operating point along the d-axis of the synchronous frame. Equation (4) shows the dependence of the plant on the flux and rotor current, in the MRAS observer the PI shall be designed to operate at full flux and rated load conditions. The PI controller was tuned such that a closed-loop bandwidth of $\omega_n = 37.6\, rad/s$ (6 Hz) and damping ratio $\xi = 0.755$ were obtained.

III. Stator Flux Voltage Model Design

The voltage model in the MRAS observer as expressed in (1) requires the use of a pure integrator which in practice suffers from drift. This section analyzes the effect of the DC offsets on the ideal stator flux output from the voltage model and reviews various algorithms proposed in literature to compensate for this effect. These algorithms were modified to operate with a DFIM system.

A. Analysis of the effect of DC offsets in the Voltage Model

DC offsets are introduced in the voltage model through voltage and current measurements causing an additional flux offset component to exist in (1). This results in the drifting of Ψ_{S_α} and Ψ_{S_b}, therefore resulting in the incorrect operation of the MRAS observer.

B. Voltage model Band-pass Filter (BPF) Approximation

One typical solution applied in literature [8-10] to remove the DC offsets in the voltage model for a MRAS observer applied to a DFIM is to use a BPF to approximate the response of a pure integrator. Given that for a grid-connected DFIM the frequency of the stator voltages and currents is fixed to that of the supply such an approximation can be used.

A second order passive BPF was designed to approximate the pure integrator, with corner frequencies at $\omega_1 = 5.026\, rad/s$ (0.8 Hz) and $\omega_2 = 5.969\, rad/s$ (0.95Hz). Due to the nature of the frequency response of the second order band-pass filter, the corner frequencies should be as low as possible in order to minimize the difference in response from that of the pure integrator. The above design achieved the lowest frequencies at which no drift in the output of the voltage model. Although this paper only considers simulation of the system, this was confirmed on a 1.5 kW DFIM experimental setup (Table II).

The frequency responses of the pure integrator and BPF approximation were analyzed at a frequency of 314.159 rad/s (50 Hz). The difference in the magnitude of the two responses is negligible however a difference in phase of 2.07° was found with the above filter design. This phase difference will be reflected as an error in the rotor angle estimate.

C. Drift Compensator and DC offset Compensator (DDCOC)

Most techniques employed to eliminate DC offsets without introducing phase errors rely on the principle of correcting the input to the pure integrator through a feedback mechanism [11, 12]. In [11] the correction mechanism makes use of two compensators:

1) Flux Drift Compensator

2) Flux DC Offset Compensator

The compensators in [11] were developed for a standard induction motor for its Rotor Flux Estimator. In this paper the compensators were adapted for a Stator Flux Estimator as shown in Fig. 3. In the flux drift compensator a voltage offset calculation is performed and fed back to the summation point in the same block. The voltage offset calculation is given by:

$$v_{offset} = \frac{\hat{\Psi}_{S1_{max}} + \hat{\Psi}_{S1_{min}}}{2\Delta t} \qquad (10)$$

Where $\hat{\Psi}_{S1_{max}}$ and $\hat{\Psi}_{S1_{min}}$ are the maximum and minimum fluxes in $\hat{\Psi}_{S1_\alpha}$ and $\hat{\Psi}_{S1_\beta}$, and Δt is the time period between maximum and minimum points.

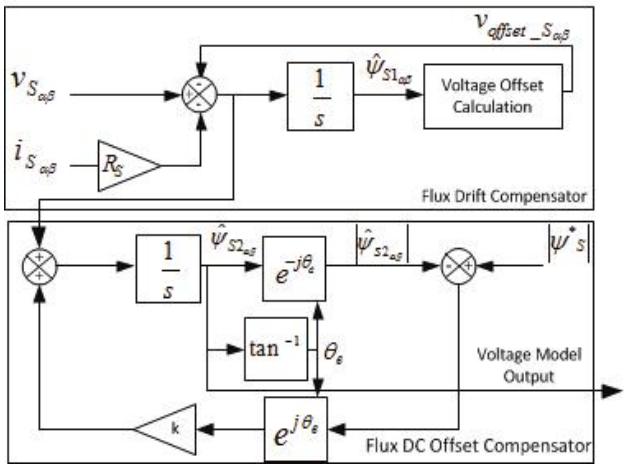

Fig. 3. Voltage Model with Drift Compensator and DC Offset Compensator (DDCOC)

Since SFO is used, tracking of the maximum and minimum points of $\hat{\Psi}_{S1_\alpha}$ and $\hat{\Psi}_{S1_\beta}$, is done by sampling at particular values of the stator flux angle θ_e obtained from the stator flux voltage model output.

The DC Offset Compensator [12] uses the output of the summation point in the Drift Compensator as shown in Fig. 3 in order to compensate any offset which is still present. This compensator calculates the voltage offset as shown below.

$$v_{off2} = k\left(\left|\Psi^*_{S_{\alpha\beta}}\right| - \left|\hat{\Psi}_{S2_{\alpha\beta}}\right|\right) e^{j\theta_e} \qquad (11)$$

Where k is the gain in the feedback path, $\left|\Psi^*_{S_{\alpha\beta}}\right|$ is the magnitude of the ideal flux, $\left|\hat{\Psi}_{S2_{\alpha\beta}}\right|$ is the magnitude of flux output from the integrator and θ_e is the stator flux angle. The voltage offset is fed back to the summation block prior to the integrator in the same block. The flux output from the DC Offset Compensator block is used as the output of the voltage model.

D. Proportional Integral (PI) Feedback Compensator

Another compensation technique using a flux feedback mechanism was developed in [13]. In this system, the DC the DC offset is eliminated by feeding back the stator flux at the output of the voltage model through a PI controller as shown in Fig. 4. The required stator flux is represented by a reference flux $\Psi^*_{S_{\alpha\beta}} = \left|\Psi^*_{S_{\alpha\beta}}\right| \angle\theta_e$, where the magnitude is based on the expected stator flux of the machine. The flux offset in the $\alpha\beta$-frame can be expressed as:

$$\Psi_{Sof_{\alpha\beta}} = \Psi_{S_{\alpha\beta}}\left(1 - \frac{\left|\Psi^*_{S_{\alpha\beta}}\right|}{\left|\Psi_{S_{\alpha\beta}}\right|}\right) \qquad (12)$$

$\Psi_{Sof_{\alpha\beta}}$ is passed through a PI controller to obtain the voltage offset estimate $v_{Sof_{\alpha\beta}}$ which is fed back to the summation point prior to the pure integrator. The system plant is shown below:

$$CLTF(s) = \frac{s^2}{s^2 + (K_p s + K_i)\chi} \qquad (13)$$

where $\chi = \left(1 - \frac{\left|\Psi^*_{S_{\alpha\beta}}\right|}{\left|\Psi_{S_{\alpha\beta}}\right|}\right)$

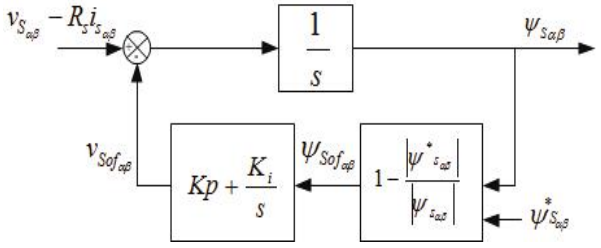

Fig. 4. Voltage Model with PI feedback compensator

The suggested tuning parameters [13] for the PI controller are $Kp = 2\xi\omega_0$ and $Ki = \omega_0^2$. Where ω_0 is calculated by $\omega_0 = \frac{\omega_{min}}{d}$, and ω_{min} is the minimum stator frequency. The optimum response observed via simulation are with $d = 4$ and $\xi = 0.85$ in agreement with the constraints suggested in [13] .

E. Modified Integrator Compensator

In [14] a modification to the pure integrator was derived using a different approach from the previous techniques as shown in [11-13]. A high-pass filter is applied in series with the pure integrator to eliminate the DC offset. Since the high-pass filter modifies the response of the pure integrator; the high-pass and pure integrator combination are multiplied by the inverse of the high-pass filter such that the resulting transfer function is equivalent to that of the integrator. The pure integrator, high-pass filter and inverse high-pass filter transfer function can be simplified into a low-pass filter form and written as:

$$\frac{dy}{dt} = \big(1 - j\lambda sign(\omega)\big)u - \lambda|\omega|y \qquad (14)$$

Where *'u'* and *'y'* are the input and output of the low-pass filter, ω is the angular frequency and λ is a tuning constant. Integrating both sides in (14) with respect to time yields:

$$y = \int\{\big(1 - j\lambda\, sign(\omega)\big)u - \lambda|\omega|y\}\, dt \qquad (15)$$

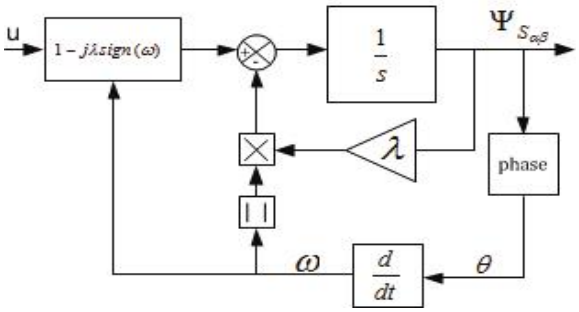

Fig. 5. Voltage Model with Modified Integrator compensator

The input to the modified integrator to be used in the stator flux voltage model as shown in Fig. 5 is:

$$u = \left(v_{S_\alpha} + j\, v_{S_\beta}\right) - R_s(i_{S_\alpha} + j i_{S_\beta}) \qquad (16)$$

Hence the flux outputs in the stationary alpha-beta frame can be expressed as:

$$\Psi_{S_\alpha} = \int\left(v_{S_\alpha} - R_S i_{S_\alpha}\right) + \lambda sign(\omega)\left(v_{S_\beta} - R_S i_{S_\beta}\right) - \lambda|\omega|\Psi_{S_\alpha}\, dt \qquad (17)$$

$$\Psi_{S_\beta} = \int\left(v_{S_\beta} - R_S i_{S_\beta}\right) + \lambda sign(\omega)\left(v_{S_\alpha} - R_S i_{S_\alpha}\right) - \lambda|\omega|\Psi_{S_\beta}\, dt \qquad (18)$$

IV. Results

The simulations for the DFIM with MRAS observer for the various Stator Voltage Models discussed in section III were performed using Simulink© and MATLAB©. The synchronous frame reference currents for rated operation of the motor in Table II are $i_{R_d}^* = 2.82\ A$ and $i_{R_q}^* = 2.39\ A$. The grid-connected DFIM is driven by a DC machine with an initial speed of 1500 rpm and its rated d and q current were applied at 0.5 s and 1 s respectively. The performance of the system was tested when sensorless control was enabled and also during speed demands which ramp down and up to 1000 rpm and 2000 rpm respectively. Since typical wind speeds in wind energy conversion systems (WECS) range from 1000 to 2000 rpm [15] the initial estimated rotor frequency of the MRAS observer was set to 1500 rpm.

Results with the BPF approximation are shown in Figs. 6 to 8. The MRAS observer is switched on at 2 s and the estimated angle and frequency are used for sensorless control at 3s. The actual and estimated shaft speeds are shown in Fig. 6, the response of the synchronous frame currents is shown in Fig. 7. The error between the actual and estimated rotor angle is shown in Fig. 8.

Results for simulations under the same operating conditions with the combined Flux Drift Compensator and Flux DC Compensator (Fig. 3) are shown in Figs. 9 to 11. The results obtained for the Modified Integrator Compensator (Fig. 5) are similar to Figs. 9 to 11 and have not been included in this paper.

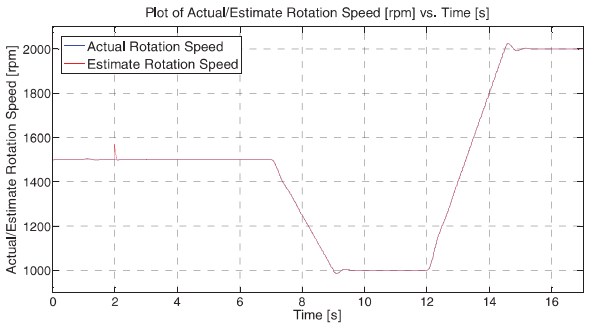

Fig. 6. Actual/Estimated Shaft Speed (rpm) vs. Time (s) with BPF approximation

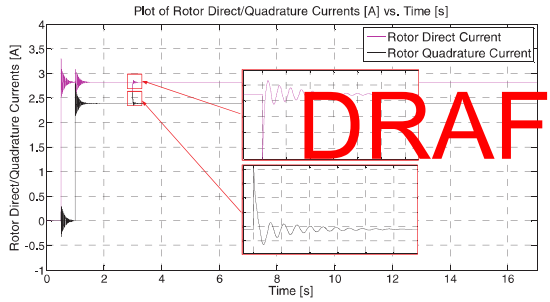

Fig. 7. Synchronous dq currents (A) vs. Time (s) with BPF approximation

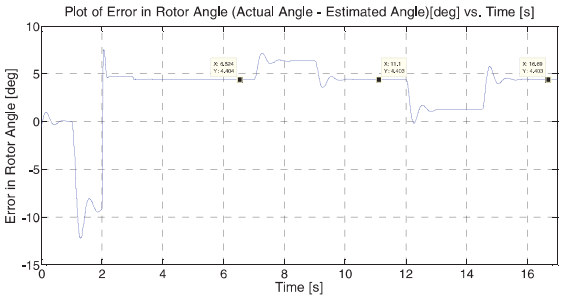

Fig. 8. Error in estimated rotor angle (degrees) vs. Time (s) with BPF approximation

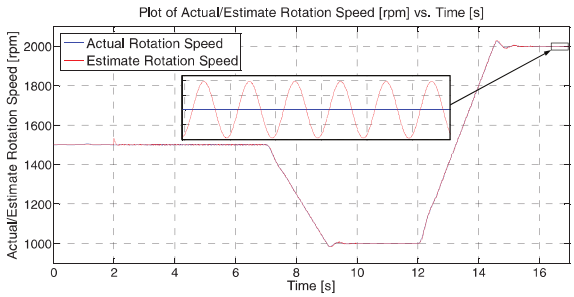

Fig. 9. Actual/Estimated Shaft Speed (rpm) vs. Time (s) with Drift Compensator and DC Compensator

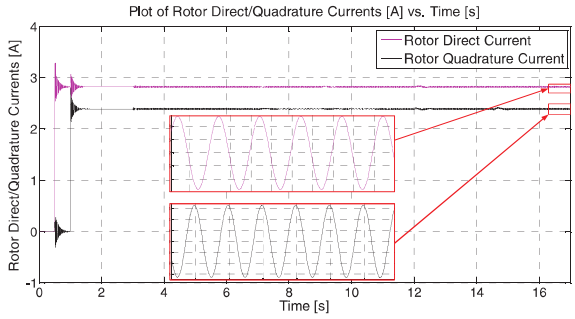

Fig. 10. Synchronous dq currents (A) vs. Time (s) with Drift Compensator and DC Compensator

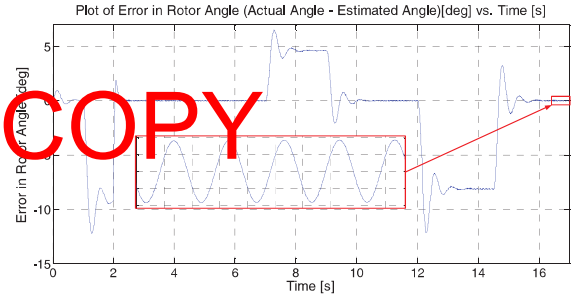

Fig. 11. Error in estimated rotor angle (degrees) vs. Time (s) with Drift Compensator and DC Compensator

Results with the PI Feedback Compensator are shown in Figs. 12 to 14. The MRAS observer is switched on at 2 s and the estimated angle and frequency are used for sensorless control at 7 s. The actual and estimated shaft speeds are shown in Fig. 12, the response of the synchronous frame currents is shown in Fig. 13 and the error between the actual and estimated rotor angles is shown in Fig. 14.

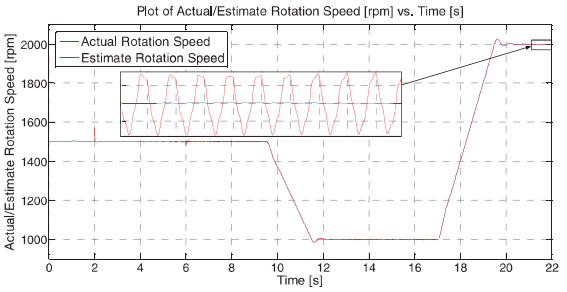

Fig. 12. Actual/Estimated Shaft Speed (rpm) vs. Time (s) with PI feedback Compensator

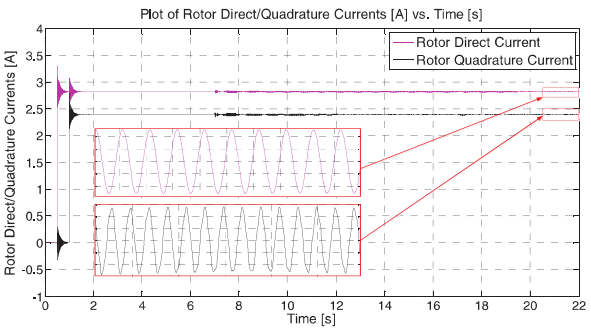

Fig. 13. Synchronous dq currents (A) vs. Time (s) with PI feedback Compensator

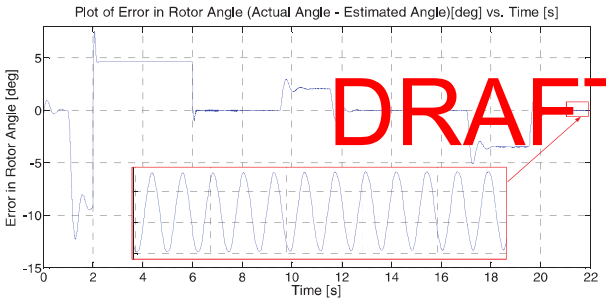

Fig. 14. Error in estimated rotor angle (degrees) vs. Time (s) with PI feedback compensator

Table I summarises the results obtained by the different methods used. The table shows the amplitudes of the oscillations in the estimated speed, synchronous currents and error in the estimated rotor angle obtained in steady-state operation. The tabulated results were used for comparison of the performance of the various methods simulated.

TABLE I

AMPLITUDES OF OSCILLATIONS IN RESULTS

Compensation Technique	Estimated Speed (rpm)	Max. i_{R_d}/i_{R_q} (A)	Estimated Rotor Angle Error $\theta_R - \hat{\theta}_R$ (degrees)
Flux compensator + Drift compensator	0.90	0.016	0.036
PI feedback	0.34	0.005	0.01
Modified Integrator	0.75	0.015	0.03

V. COMMENTS AND CONCLUSIONS

The paper presented various model based sensorless algorithms for the sensorless control of a DFIM used in wind energy conversion. The different voltage methods were compared by analysis of the oscillations at steady-state in the speed and angle estimate. The voltage model based on the BPF approximation obtained the estimated speed shown in Fig. 6 which shows a speed transient from 1500 to 1000 back to 2000 rpm. This speed range was investigated since it's the most common in wind based systems. When the rotational shaft speed is constant at 2000 rpm, the error between the actual and estimated angles for the BPF approximation is constant at 4.403° as shown in Fig. 8. This angle difference will result in oscillations in the synchronous frame currents (Fig. 7) when the system is switched to sensorless mode of operation. In order to reduce the error in the estimated rotor angle, the BPF in the MRAS loop has to be replaced by voltage models which apply compensation techniques to reduce the error further.

The alternative voltage models using compensation were found to reduce the error in the rotor angle to a value close to 0°. The results for the DDCOC and the PI feedback compensator systems are shown in Fig. 11 and Fig. 14 respectively. These two techniques also introduced minor oscillations in the speed estimates (Table I). These oscillations will be reflected in the rotor position estimate and consequently in the steady state synchronous frame currents. The transient response in the currents when switching to sensorless control is improved in all of the compensator based voltage models when compared to the BPF approximation as shown in Fig. 10 and Fig. 13. From the studies carried out it was found that the estimated speed of the PI Feedback Compensator (Fig. 12) performed best at steady-state and achieved the smallest oscillations (Table I). The oscillations introduced in the d and q currents and in the error in the estimated rotor angle are also smallest for this technique. The drawback of the PI feedback compensator is the increased settling time introduced in the angle/speed estimates which results in a delay in the sensorless changeover.

All the alternative voltage models presented were shown to significantly reduce the error in the rotor angle when compared to the BPF approximation. It was found that for the optimum performance at steady state, the PI based system performed best, however if the system requires changing to sensorless operation in a shorter time, the Drift and DC Offset compensator can be applied with similar performance.

TABLE II

DFIM PARAMETERS

Parameter	Stator	Rotor
Power	1.5 kW	-
Phase voltage, current	210 V, 4.5A	150 V, 3.7 A
Resistance	1.25 Ω	1.60 Ω
Frequency	50 Hz	-
Leakage Inductance	10.83 mH	1.54 mH
Mutual Inductance	143.42 mH	
Turns Ratio (stator to rotor)	1.32	

ACKNOWLEDGMENT

The authors would like to acknowledge the contributions of the support technical staff at the Department of Industrial Electrical Power Conversion, University of Malta. This work as supported by the Strategic Educational Pathways Scholarship (STEPS) programme Malta.

REFERENCES

[1] E. Tremblay, S. Atadye, and A. Chandra, "Comparative Study of Control Strategies for the Doubly Fed Induction Generation in Wind Energy Conversion Systems: A DSP-Based Implementation Approach," *IEEE Trans. Sustainable Energy,* vol. 2, pp. 288-299, Jul. 2011.

[2] S. Li, T. A. Haskew, K. A. Williams, and R. P. Swatloski, "Control of DFIG Wind Turbine Direct-Current Vector Control Configuration," *IEEE Trans. Sustainable Energy,* vol. 3, pp. 1-11, Jan. 2012.

[3] M. S. Carmeli, F. Castelli-Dezza, M. Iacchetti, and R. Perini, "Effects of Mismatched Parameters in MRAS Sensorless Doubly Fed Induction Machine Drives," *Power Electronics, IEEE Transactions on,* vol. 25, pp. 2842-2851, 2010.

[4] K. Spiteri, C. S. Staines, and M. Apap, "A three phase to three phase bidirectional power matrix converter," in *Communications, Control and Signal Processing, 2008. ISCCSP 2008. 3rd International Symposium on*, 2008, pp. 1404-1408.

[5] K. Spiteri, C. S. Staines, and M. Apap, "Power control of doubly fed induction machine using a rotor side matrix converter," in *Industrial Electronics (ISIE), 2010 IEEE International Symposium on*, 2010, pp. 1445-1450.

[6] K. Spiteri, C. S. Staines, and M. Apap, "Control of doubly fed induction machine using a matrix converter," in *MELECON 2010 - 2010 15th IEEE Mediterranean Electrotechnical Conference*, 2010, pp. 1297-1302.

[7] C. Schauder, "Adaptive Speed Indentification for Vector Control of Induction Motors without Rotational Transducers," *IEEE Trans. Ind. Appl.,* vol. 28, pp. 1054-1061, 1992.

[8] R. Cardenas, R. Pena, G. Asher, J. Clare, and J. Cartes, "MRAS Observer for Doubly Fed Induction Machines," *IEEE Trans. Energy Convers.,* vol. 19, Jun. 2004.

[9] R. Cardenas, R. Pena, J. Clare, G. Asher, and J. Proboste, "MRAS Observers for Sensorless Control of Doubly-Fed Induction Geneartors," *IEEE Trans. Power Electron.,* vol. 23, pp. 1075-1084, May 2008.

[10] R. Cardenas, R. Pena, J. Proboster, G. Asher, and J. Clare, "MRAS Observer for Sensorless Control of Standalone Doubly Fed Induction Generators," *IEEE Trans. Energy Convers.,* vol. 20, pp. 710-718, Dec. 2005.

[11] Q. Gao, C. S. Spiteri, G. M. Asher, and M. Sumner, "Sensorless speed operation of cage induction motor using zero drift feedback integration with MRAS observer," presented at the European Conference on Power Electronics and Applications, Dresden, Germany, Aug. 2005.

[12] J. Holtz and J. Quan, "Sensorless Vector Control of Induction Motors at Very Low Speed Using a Nonlinear Inverter Model and Parameter Identification," *IEEE Trans Ind. Appl.,* vol. 38, pp. 1087-1095, Aug. 2002.

[13] C. Lascu and G. D. Andreescu, "Sliding-Mode Observer and Improved Integrator with DC-Offset Compensation for Flux Estimation in Sensorless-Controlled Induction Motors," *IEEE Trans. Ind. Electron.,* vol. 53, pp. 785-794, Jun. 2006.

[14] M. Hinkkanen and J. Luomi, "Modified Integrator for Voltage Model Flux Estimation of Induction Motors," *IEEE Trans. Ind. Electron.,* vol. 50, pp. 818-820, Aug. 2003.

[15] G. Abad, J. Lopez, M. A. Rodriguez, L. Marroyo, and G. Iwanski, "Introduction to A Wind Energy Generation System," in *Doubly Fed Induction Machine - Modelling and Control for Wind Energy Generation*, L. Hanzo, Ed., ed New Jersey: John Wiley & Sons, 2011.